

# Gas surface density, star formation rate surface density, and the maximum mass of young star clusters in a disk galaxy. II. The grand-design galaxy M 51

Rosa A. González-Lópezlira<sup>1,2</sup>, Jan Pflamm-Altenburg<sup>1</sup>, & Pavel Kroupa<sup>1</sup>

## ABSTRACT

We analyze the relationship between maximum cluster mass, and surface densities of total gas ( $\Sigma_{\text{gas}}$ ), molecular gas ( $\Sigma_{\text{H}_2}$ ), neutral gas ( $\Sigma_{\text{HI}}$ ) and star formation rate ( $\Sigma_{\text{SFR}}$ ) in the grand design galaxy M 51, using published gas data and a catalog of masses, ages, and reddenings of more than 1800 star clusters in its disk, of which 223 are above the cluster mass distribution function completeness limit. By comparing the 2-D distribution of cluster masses and gas surface densities, we find for clusters older than 25 Myr that  $M_{3\text{rd}} \propto \Sigma_{\text{HI}}^{0.4 \pm 0.2}$ , where  $M_{3\text{rd}}$  is the median of the 5 most massive clusters. There is no correlation with  $\Sigma_{\text{gas}}$ ,  $\Sigma_{\text{H}_2}$ , or  $\Sigma_{\text{SFR}}$ . For clusters younger than 10 Myr,  $M_{3\text{rd}} \propto \Sigma_{\text{HI}}^{0.6 \pm 0.1}$ ,  $M_{3\text{rd}} \propto \Sigma_{\text{gas}}^{0.5 \pm 0.2}$ ; there is no correlation with either  $\Sigma_{\text{H}_2}$  or  $\Sigma_{\text{SFR}}$ . The results could hardly be more different than those found for clusters younger than 25 Myr in M 33. For the flocculent galaxy M 33, there is no correlation between maximum cluster mass and neutral gas, but we have determined  $M_{3\text{rd}} \propto \Sigma_{\text{gas}}^{3.8 \pm 0.3}$ ;  $M_{3\text{rd}} \propto \Sigma_{\text{H}_2}^{1.2 \pm 0.1}$ ;  $M_{3\text{rd}} \propto \Sigma_{\text{SFR}}^{0.9 \pm 0.1}$ . For the older sample in M 51, the lack of tight correlations is probably due to the combination of the strong azimuthal variations in the surface densities of gas and star formation rate, and the cluster ages. These two facts mean that neither the azimuthal average of the surface densities at a given radius, nor the surface densities at the present-day location of a stellar cluster represent the true surface densities at the place and time of cluster formation. In the case of the younger sample, even if the clusters have not yet traveled too far from their birthsites, the poor resolution of the radio data compared to the physical sizes of the clusters results in measured  $\Sigma$ s that are likely quite diluted compared to the actual densities relevant for the formation of the clusters.

*Subject headings:* galaxies: star clusters — galaxies: ISM — galaxies: spirals — stars: formation — galaxies: individual (M 51, NGC 5194)

## 1. Introduction

This is the second in a series of papers devoted to investigate whether the maximum young cluster masses observed in a galaxy reflect physical processes that determine them or if, instead, they constitute an effect of random sampling statistics.

A correlation between gas surface density and embedded maximum cluster mass (i.e.,  $M_{\text{ecl,max}} \propto \Sigma_{\text{gas}}^{3/2}$ ) has been proposed as an ansatz to explain

the existence of the  $\text{H}\alpha$  cut-off in disk galaxies, while at the same time, as can be inferred from UV data, there is no actual star formation cut-off (Pflamm-Altenburg & Kroupa 2008; Pflamm-Altenburg et al. 2009). Similarly, a correlation  $M_{\text{ecl,max}} \propto \Sigma_{\text{SFR}}^\eta$  has been proposed by Billett et al. (2002) and Larsen (2002), arising from the star formation law ( $\Sigma_{\text{SFR}} \propto \Sigma_{\text{gas}}^{1.4}$  Kennicutt 1998), in conjunction with the assumption of pressure equilibrium between the ambient ISM and the cluster-forming cloud cores. In this case,  $2/3 \leq \eta \leq 2$ , with the lower value expected for equal (volume) density clusters, and the higher one for clusters with equal size (Larsen 2002).

In the first paper of the series (González-Lópezlira et al.

<sup>1</sup>Argelander Institut für Astronomie, Universität Bonn, Auf dem Hügel 71, D-53121 Bonn, Germany

<sup>2</sup>On sabbatical leave from the Centro de Radioastronomía y Astrofísica, UNAM, Campus Morelia, Michoacán, México, C.P. 58089; r.gonzalez@crya.unam.mx

2012), we analyzed radially averaged distributions of gas surface densities and of cluster masses in the flocculent galaxy M 33. Here, we study the grand-design galaxy M 51. Star cluster data are presented in Section 1, and ISM data in Section 2; both cluster and gas data are taken from the literature. The results and a comparison with M 33 are discussed in Section 3. Section 4 contains our summary and conclusions.

## 2. Star cluster data

We rely on two catalogs of star clusters brighter than  $V_{F555W} = 23$  mag, detected by Hwang & Lee (2008), based on Hubble Space Telescope (*HST*) Advanced Camera for Surveys (ACS) observations acquired by the Hubble Heritage Team. Hwang & Lee compiled two catalogs, one of 2224 “Class 1” clusters, that appear circular and well isolated, and one with 1388 “Class 2” clusters, which have elongated or irregular shapes and/or close neighbors. These original catalogs list, among other properties, cluster RA and DEC, half-light radius  $R_{\text{eff}}$ ,  $(B - V)$  and  $(V - I)$  colors, aperture corrected  $V$  mag, and photometric errors, all in the *HST* equivalent of the Johnson system. From the recovery of artificial clusters, Hwang & Lee (2008) determined that the completeness of clusters with  $V < 23$  mag is higher than 80%, regardless of the clustering properties of the field.

Subsequently, Hwang & Lee (2010) calculated masses, ages, and reddening for the clusters, via the comparison of their broad band<sup>1</sup> spectral energy distributions (SEDs) with theoretical SEDs derived from the Bruzual & Charlot (2003) stellar population synthesis models. The models used by Hwang & Lee (2010) have a Salpeter initial mass function (IMF), with lower and upper mass cut-offs of  $0.1 M_{\odot}$  and  $100 M_{\odot}$ , respectively; ages between 1 Myr and 15 Gyr; and solar metallicity. Each one of the 182 model spectra was reddened by  $E(B - V)$  values between 0.0 and 0.6 in 40 0.015 mag steps.<sup>2</sup> The age and reddening of each cluster were determined simultaneously, from a  $\chi^2$

<sup>1</sup> The Hubble Heritage ACS data set for M 51 comprises images in the  $F435W$ ,  $F555W$ , and  $F814W$  filters. Hwang & Lee (2010) complemented these with archival  $F336W$  Wide Field Planetary Camera 2 (WFPC2) data.

<sup>2</sup>This range in color excess includes the values obtained for M 51 clusters by previous studies; most clusters have  $E(B -$

fit of the reddened model SEDs to the photometric data. The original catalogs were thus reduced to 1125 Class 1 and 835 Class 2 objects with acceptable fits. For each cluster, a mass was finally assigned from the mass to light ratio  $M/L_V$  of the best-fit model and the  $V$ -band cluster magnitude, taking the measured extinction into account and adopting a distance to M 51 of 8.4 Mpc (Feldmeier et al. 1997).<sup>3</sup> The Hwang & Lee (2010) catalogs list, for each cluster, log age and errors, log mass, color excess and errors, and  $\chi^2$  value of the best-fit. These catalogs do not provide an error in the mass determination. One possible estimate is given by the  $M/L_V$  ratios at the minimum and maximum ages (the age minus and plus its error, respectively) of each cluster. Except for 24 (out of 1960) clusters (half of them less massive than  $5 \times 10^3 M_{\odot}$ ), this error is smaller than 0.15 dex (35% of the mass) in all cases. The dominant source of error is probably the uncertainty in the distance modulus (0.6 mag, or a factor of  $\lesssim 2$  in mass). It would affect all the masses equally, though, so it would not change the exponent of any relationship between cluster mass and gas or SFR surface density.

The age distribution of the clusters shows three peaks, that likely signpost bursts of enhanced star formation rate, respectively, at stellar ages of  $\approx 5$ , 100, and 200 Myr. The two older starbursts are better traced by the detected Class 1 objects, which have masses ranging from  $\approx 3 \times 10^3$  to  $\gtrsim 1 \times 10^6 M_{\odot}$ . Conversely, detected clusters in the recent burst belong mostly to Class 2, with significantly lower masses, between  $\approx 600$  and  $4 \times 10^4 M_{\odot}$ .

## 3. ISM data

Since M 51 is a grand-design spiral with large azimuthal variations of gas surface density, a two-dimensional approach is required, as opposed to a comparison of individual cluster masses with radial gas profiles, that was adequate for M 33.

We use the HI map of M 51 data from Rots et al. (1990); it was originally acquired with the Very Large Array (VLA) and has a spatial resolution of  $13''$ . We derive the molecular gas

$V) < 0.1$  (Lee et al. 2005).

<sup>3</sup> At this distance,  $1'' = 40.7$  pc;  $R_{25}$ , the galactocentric distance of the isophote with surface brightness in the  $B$ -band  $\mu_B = 25$  mag  $\square''^{-1}$ , is 13.7 kpc or  $5'.6$ .

surface density distribution from the  $^{12}\text{CO}$  2–1 mosaic obtained by Schuster et al. (2007) with the IRAM-30 m telescope; it has a resolution of  $11''$ . Finally, to calculate the SFR surface density distribution we rely on the total power 20 cm radio continuum image published by Fletcher et al. (2011); it has a resolution of  $15''$ , and was produced from VLA C- and D-array data.

In order to get the  $\text{H}_2$ , HI, and SFR surface densities from the integrated intensity maps, we follow the same procedures as Schuster et al. (2007). At a given position in M 51, the neutral gas surface density  $\Sigma_{\text{HI}} = m_{\text{H}}N(\text{HI}) \cos i$ , where  $m_{\text{H}}$  is the hydrogen atomic mass and  $i = 20^\circ$  is the inclination angle of M 51; assuming optically thin emission,  $N(\text{HI}) = 1.82 \times 10^{18} \int T_{\text{mb}} dv / (\text{K km s}^{-1})\text{cm}^{-2}$ . Likewise, we obtain the molecular gas surface density as  $\Sigma_{\text{H}_2} = 2 m_{\text{H}}N(\text{H}_2) \cos i$ . Schuster et al. (2007) assume a CO 2-1/1-0 intensity of 0.8, and a constant CO to  $\text{H}_2$  conversion factor,  $X$ , 1/4 that of the Milky Way (MW), with  $X_{\text{MW}} = 2.3 \times 10^{20} \text{ cm}^{-2} (\text{K km s}^{-1})^{-1}$ , such that the molecular hydrogen column density is  $N(\text{H}_2) = 0.25 X_{\text{MW}}(1/0.8) \int T_{\text{mb}}(\text{CO}(2-1)) dv$ , where  $T_{\text{mb}}$  is the main beam brightness temperature. The total gas surface density is  $\Sigma_{\text{gas}} = 1.36(\Sigma_{\text{H}_2} + \Sigma_{\text{HI}})$ , so as to include helium. Again, following Schuster et al. (2007), we derive  $\Sigma_{\text{SFR}}$  from the 20 cm radio continuum data.<sup>4</sup> The 20 cm non-thermal radio continuum is due to synchrotron radiation by supernovae-accelerated cosmic rays; it hence traces recent star formation, and has a strong correlation with the far-infrared (FIR; e.g., Helou et al. 1985).<sup>5</sup> At the position of each star cluster, gas surface densities are obtained from the HI,  $\text{H}_2$ , and 20 cm mosaics averaging, respectively, the emission over  $20 \times 20 \square''$  ( $\approx 820 \times 820 \text{ pc}^2$ ),  $18 \times 18 \square''$  ( $\approx 730 \times 730 \text{ pc}^2$ ), and  $18 \times 18 \square''$ .<sup>6</sup>

<sup>4</sup> $\Sigma_{\text{SFR}} = 1.53 \times 10^5 \frac{S_{20\text{cm}} \cos(i)}{[\text{Jy beam}^{-1}]} M_{\odot} \text{pc}^{-2} \text{Gyr}^{-1}$ .

<sup>5</sup>  $\Sigma_{\text{SFR}}$  can be readily derived from FIR emission, given that a significant amount of it is due to reprocessing by dust of light from young stars; FIR emission also has the advantage that it does not need to be corrected for extinction. In fact, Rosa-González et al. (2002) find that SFRs obtained at optical and UV wavelengths are often overcorrected for extinction, since stellar Balmer absorption contaminates emission lines; optical/UV and FIR/mm SFR estimators agree well once this effect is taken into account.

<sup>6</sup> The limit is imposed by the pixel size of the CO image, i.e.,  $6''$  on the side; the smallest area over which we can average the flux is a subarray of  $3 \times 3$  pixels (sides of subarrays must

Ninety-five of the clusters in the sample have coordinates that fall outside of the borders of the radio images, so that only 1865 objects can be compared with the gas and SFR densities at their location in the M 51 disk.

## 4. Results

Hwang & Lee (2008) find that the completeness distribution is quite similar for both Class 1 and Class 2 clusters. Since cluster brightness in the optical diminishes with age, the completeness limit of the cluster mass function depends on cluster age. Based on their photometric completeness limits, Hwang & Lee determine that conservative limits over which their mass functions are not affected by incompleteness are  $\approx 5 \times 10^3 M_{\odot}$  for clusters younger than  $10^7$ , and at least  $1 \times 10^5 M_{\odot}$  for clusters between 100 and 250 Myr.

### 4.1. The bursts 100 and 250 Myr ago

We will first work with the 167 clusters in the catalogs with at least  $10^5 M_{\odot}$ , ages between 40 and 400 Myr,<sup>7</sup> and detected CO, HI, and 20 cm emission at their present locations. Chandar et al. (2010) and Chandar et al. (2011) find that the cluster mass function is approximately independent of age (and the age function independent of mass) for clusters younger than  $4 \times 10^8$  yr in M 83 and M 51 (Chandar et al. 2011), respectively. Similar results are found for the Magellanic Clouds (Parmentier & de Grijs 2008) and the Antenna galaxies (Fall et al. 2009). The implication is that the mass-dependent disruption timescale is  $> 2$  Gyr (Chandar et al. 2010).

We take care here to compare cluster mass with gas and SFR surface density always in bins with the same number of clusters, in order to test whether any change in maximum cluster mass is a statistical, size-of-sample effect.<sup>8</sup> We search for

have an odd number of pixels), centered on the position of each cluster. We match the elements over which we average the HI and 20 cm fluxes to this  $18'' \times 18''$  footprint as closely as is allowed by the pixel sizes of the images, respectively,  $4'' \times 4''$  (arrays with 5 pixels on the side) and  $2'' \times 2''$  (arrays of  $9 \times 9$  square pixels).

<sup>7</sup>The young tail of the age distribution of the clusters in the  $10^8$  yr old burst reaches 25 Myr, but no cluster in this group that is younger than 40 Myr makes the  $10^5 M_{\odot}$  cut.

<sup>8</sup> If clusters are drawn randomly from the same mass distribution function that declines with mass, the probability of

correlations between cluster mass, and gas and SFR surface densities of the form:

$$\log_{10} M_i = \beta'_x \log_{10} \Sigma_x + \alpha'_x, \quad (1)$$

where  $M_i$  is the mass of the  $i$ -th most massive star cluster, and  $x$  stands for HI, H2, total gas or SFR.

Figures 1, 2, 3, and 4 show log of star cluster mass versus, respectively, log of total gas, molecular gas, star formation rate, and neutral gas surface densities. The comparison is performed in bins with equal number of clusters. Bins increase from 2 (upper left panel) to 6 (lower middle panel), and the number of clusters in each bin is indicated. Instead of using the maximum cluster mass in each bin for the comparison, the median of the five most massive clusters (or the third most massive cluster,  $M_{3rd}$ ) in each bin is displayed as a filled circle; the error bars represent the interquartile range, for both mass and gas/SFR surface density. Since the uncertainty in the measurement of any individual mass is typically a factor of 2-3, the median of the 5 most massive clusters in each bin should in general be a more statistically robust indicator of any existing trend (in every bin there are always more than 5 clusters more massive than the completeness limit). There is no correlation of  $M_{3rd}$  with the surface densities of total gas,  $\Sigma_{gas}$ , molecular gas,  $\Sigma_{H2}$ , or star formation rate,  $\Sigma_{SFR}$ .

Conversely, there is a hint of a correlation with  $\Sigma_{HI}$ . The slopes ( $\beta'_{HI}$ ) and intercepts ( $\alpha'_{HI}$ ) of the fits in the bins with 3 or more points, as well as their uncertainties, are listed in Table 1. The fits' average can be expressed as  $\log_{10} M_{3rd} = (0.4 \pm 0.2) \log_{10} \Sigma_{HI} + (5.2 \pm 0.3)$ .

In order to further explore whether the intrinsic mass distribution of clusters may be changing as a function of neutral gas surface density, we perform a Kolmogorov-Smirnov (K-S) test on the 6 different subsamples presented in the bottom middle panel of Figure 4. Figure 5 shows the cumulative probability distributions and  $\Sigma_{HI}$  of each subsample, and the  $D_{j,k}$  and  $P_{j,k}$  values for every bin pair  $j, k$  are given in Table 2 (higher bin number indicates larger surface density). Assuming that sample pairs with  $P_{j,k} < 0.05$  are taken from different distribution functions with high significance, bin 1 (*red solid line*), with the smallest surface density

---

picking a massive cluster increases with the size of sample.

$\Sigma_{HI} = 6.8^{+0.8}_{-2.9} M_{\odot} \text{ pc}^{-2}$ , seems to be different from bin 6 (*orange long dashed-dotted line*), with the largest surface density  $\Sigma_{HI} = 20.9^{+9.9}_{-1.4} M_{\odot} \text{ pc}^{-2}$  ( $P_{1,6} = 0.03$ ). The mass distributions in bins 3, 4, and 5 appear to lie somewhere in between. No hard conclusion can be drawn, however, since bin 2 (*green dotted line*), with the second lowest HI surface density, is in fact indistinguishable from bin 6 ( $P_{2,6} > 0.98$  for the pair).

## 4.2. The recent burst 5 Myr ago

We now analyze the 56 clusters younger than  $10^7$  yr with mass at least  $5 \times 10^3 M_{\odot}$  and higher, and detected CO, HI, and 20 cm emission at their positions. Figures 6, 7, 8, and 9 show log of star cluster mass versus, respectively, log of  $\Sigma_{gas}$ ,  $\Sigma_{H2}$ ,  $\Sigma_{SFR}$ , and  $\Sigma_{HI}$ . Bins with indicated, equal, number of clusters again increase from 2 to 6; points are the median of the 5 most massive clusters in each bin.

As with clusters in the two older bursts, there is no correlation between  $M_{3rd}$ , and  $\Sigma_{H2}$  or  $\Sigma_{SFR}$ . The correlation with  $\Sigma_{HI}$  is tighter and has a slightly steeper slope, though, with average fit for all the bins with 3 or more points  $\log_{10} M_{3rd} = (0.6 \pm 0.1) \log_{10} \Sigma_{HI} + (3.5 \pm 0.1)$ . Moreover, there is also a hint of a correlation of  $M_{3rd}$  with the total mass surface density  $\Sigma_{gas}$ , with average fit  $\log_{10} M_{3rd} = (0.5 \pm 0.2) \log_{10} \Sigma_{gas} + (3.4 \pm 0.2)$ . Fully aware that the statistical significance might be questionable, we show nonetheless  $\log_{10}$  of *maximum* cluster mass in the bin,  $M_{max}$ , versus  $\Sigma_{HI}$  for clusters younger than  $10^7$  yr in Figure 10. The error in log mass for each cluster was determined as described previously in Section 2; the error bar in  $\Sigma_{HI}$  shows the uncertainty in the measurement at the cluster's position. The average of the fits in the bins with more than 3 points is as tight as for  $M_{3rd}$ , and consistent with it:  $\log_{10} M_{max} = (0.7 \pm 0.1) \log_{10} \Sigma_{gas} + (3.6 \pm 0.1)$ . The parameters of the fits for the younger burst can be found in Table 3.

We perform once more a K-S test on the 6 different subsamples presented in the bottom middle panel of Figure 9. The test is illustrated with Figure 11, and its numerical results are given in Table 4. Bin 1 (*red solid line*), with the smallest surface density  $\Sigma_{HI} = 6.6^{+0.5}_{-2.7} M_{\odot} \text{ pc}^{-2}$ , seems to be different, with high statistical significance, from bin 6 (*orange long dashed-dotted line*), with

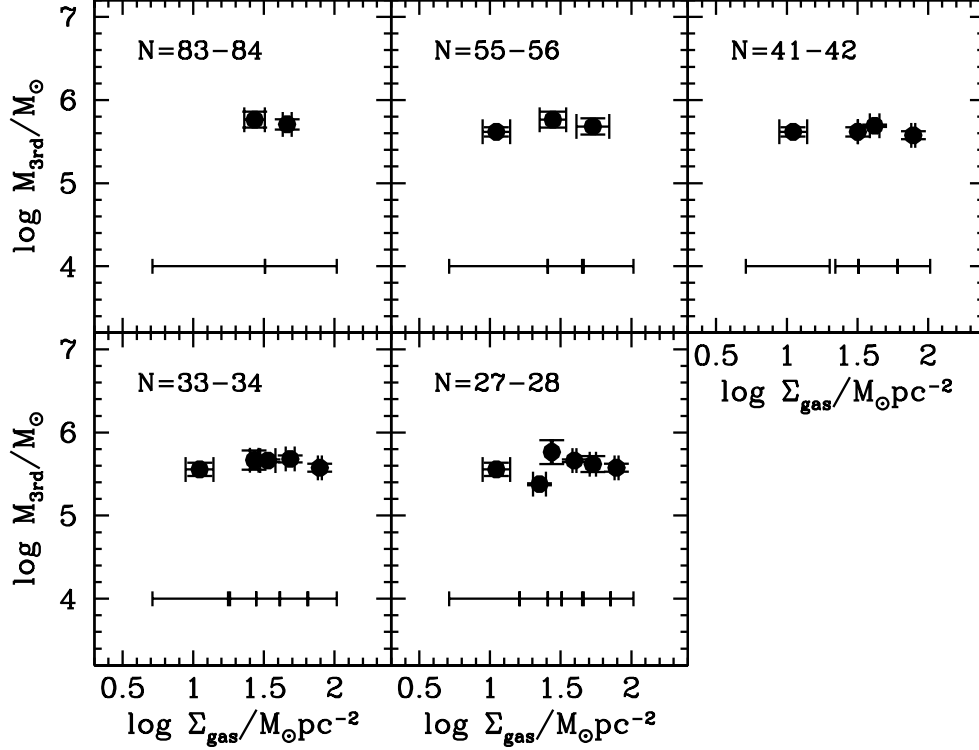


Fig. 1.— M 51, 100 and 250 Myr old bursts,  $\log_{10}$  cluster mass versus  $\log_{10}$  total gas surface density, in bins with equal number of clusters. *Filled circles*:  $M_{3rd}$ , median of 5 most massive clusters (i.e., effectively, the third most massive cluster) in the bins. Number of bins increases from 2 (upper left panel) to 6 (lower middle panel); number of clusters in each bin are indicated in the panels. The bar at the bottom of each panel shows surface density ranges of the bins.

TABLE 1

M 51, 100 AND 250 MYR OLD BURSTS. FITS TO  $\log_{10} (M_{3rd}/M_{\odot})$  VS.  $\log_{10} \Sigma_{HI}/(M_{\odot} \text{ PC}^{-2})$

$N_b$	$N_{cl}$	$\beta'_{HI}$	$\alpha'_{HI}$
3	55-56	$(0.2 \pm 0.1)$	$(5.4 \pm 0.1)$
4	41-42	$(0.2 \pm 0.1)$	$(5.4 \pm 0.1)$
5	33-34	$(0.5 \pm 0.2)$	$(5.1 \pm 0.3)$
6	27-28	$(0.7 \pm 0.3)$	$(4.8 \pm 0.3)$

NOTE.—Col. (1): number of bins. Col. (2): number of clusters in each bin. Col. (3): best-fit slope (eq. 1). Col. (4): best-fit intercept (eq. 1).

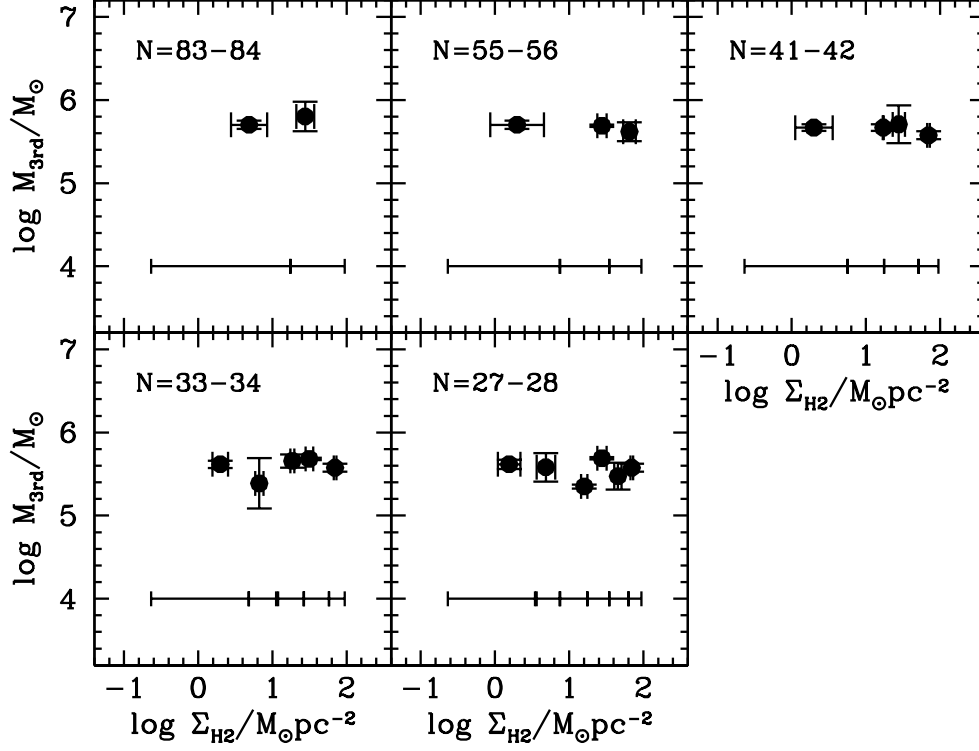


Fig. 2.— M 51, 100 and 250 Myr old bursts,  $\log_{10}$  cluster mass versus  $\log_{10}$  molecular gas surface density. Symbols as in figure 1.

TABLE 2  
K-S TEST  $D$  AND  $P$  VALUES, 100 AND 250 MYR OLD BURSTS

	$D$	$P$								
Bin	2		3		4		5		6	
1	1.53	0.0187	0.69	0.7198	0.97	0.3003	0.83	0.4903	1.44	0.0318
2			1.11	0.1687	0.83	0.4903	0.83	0.4903	0.46	0.9823
3					0.83	0.4903	0.69	0.7198	1.04	0.2337
4							0.28	1.0000	0.76	0.6100
5									0.73	0.6530

NOTE.— $D$  and  $P$  values for bin pairs. The cell in the intersection of a row  $j$  and a column  $k$  contains the  $D_{j,k}$  and  $P_{j,k}$  parameters, respectively, of the comparison between the two bins indicated in the corresponding row and column. If  $P_{j,k} < 0.05$ , the null hypothesis that the clusters in the two bins are taken from the same mass distribution function is rejected.

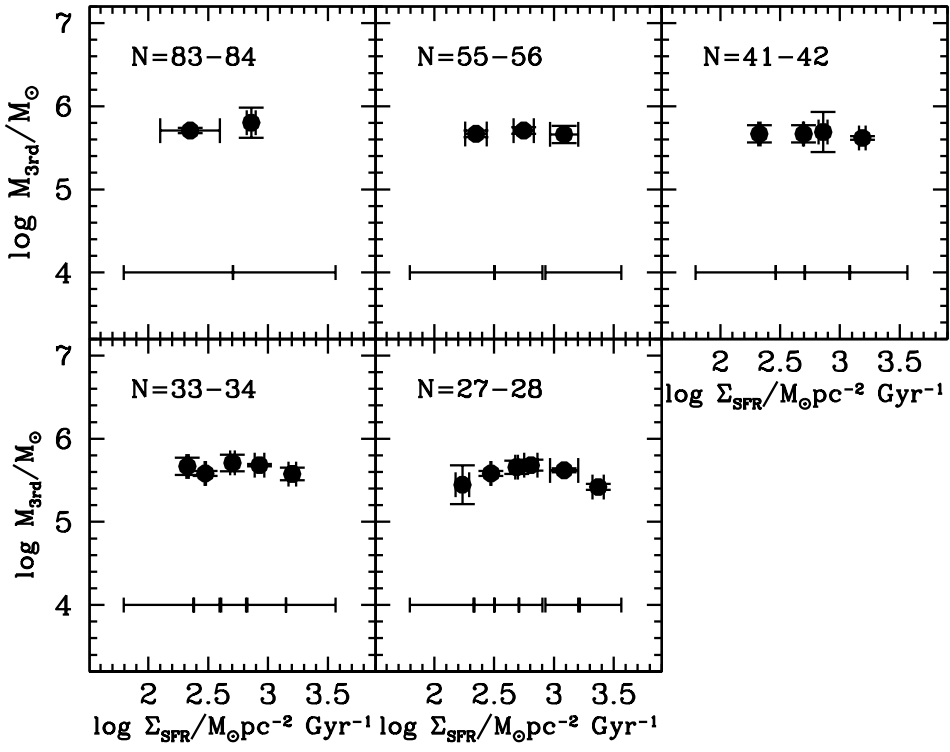


Fig. 3.— M 51, 100 and 250 Myr old bursts,  $\log_{10}$  cluster mass versus  $\log_{10}$  star formation rate surface density. Symbols as in figure 1.

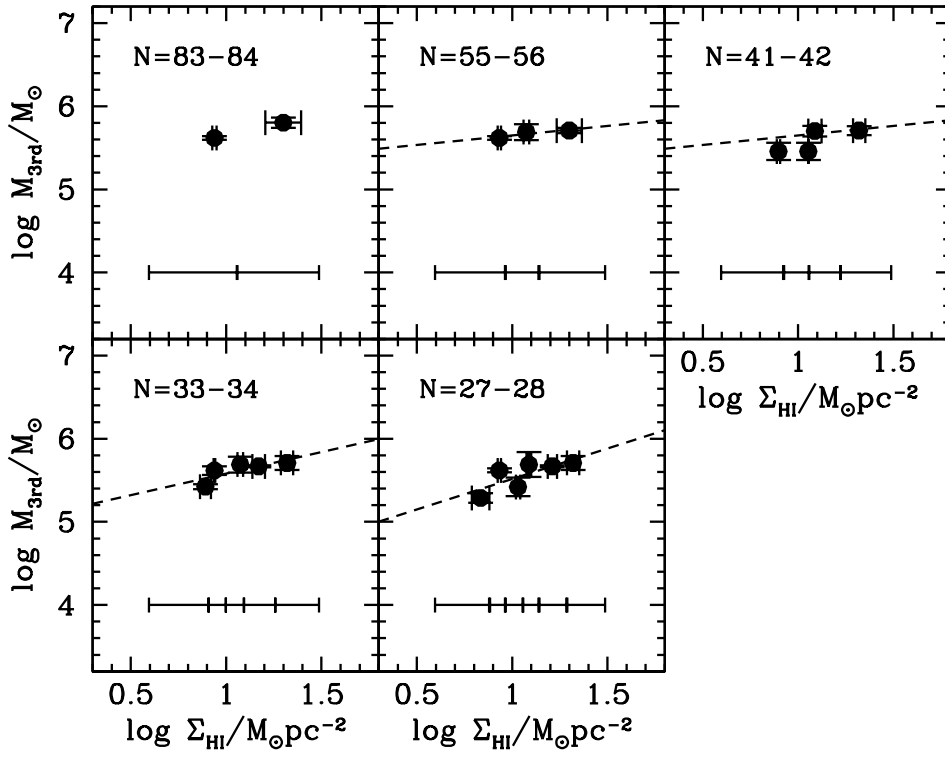


Fig. 4.— M 51, 100 and 250 Myr old bursts,  $\log_{10}$  cluster mass versus  $\log_{10}$  neutral gas surface density. *Dashed line*: linear fit. Other symbols as in figure 1.

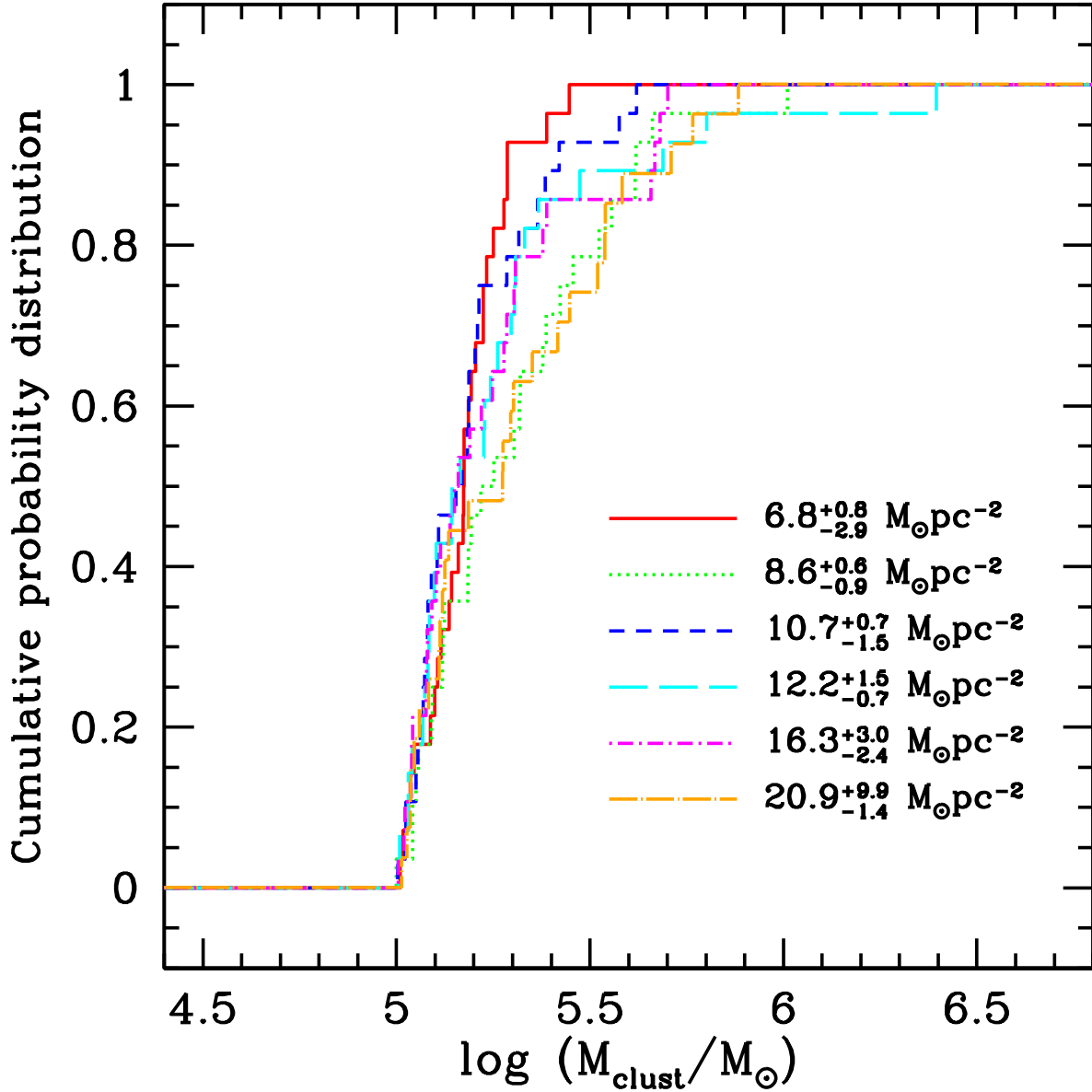


Fig. 5.— K-S test, 100 and 250 Myr old bursts. Cumulative probability distributions of mass for clusters with  $M_{\text{clust}} \geq 10^5 M_{\odot}$  in the six indicated bins of HI surface density. *Red solid line*: bin 1,  $\Sigma_{\text{HI}} = 6.8^{+0.8}_{-2.9} M_{\odot} \text{pc}^{-2}$ ; *green dotted line*: bin 2,  $\Sigma_{\text{HI}} = 8.6^{+0.6}_{-0.9} M_{\odot} \text{pc}^{-2}$ ; *blue short dashed line*: bin 3,  $\Sigma_{\text{HI}} = 10.7^{+0.7}_{-1.5} M_{\odot} \text{pc}^{-2}$ ; *cyan long dashed line*: bin 4,  $\Sigma_{\text{HI}} = 12.2^{+1.5}_{-0.7} M_{\odot} \text{pc}^{-2}$ ; *magenta short dashed-dotted line*: bin 5,  $\Sigma_{\text{HI}} = 16.3^{+3.0}_{-2.4} M_{\odot} \text{pc}^{-2}$ ; *orange long dashed-dotted line*: bin 6,  $\Sigma_{\text{HI}} = 20.9^{+9.9}_{-1.4} M_{\odot} \text{pc}^{-2}$ .

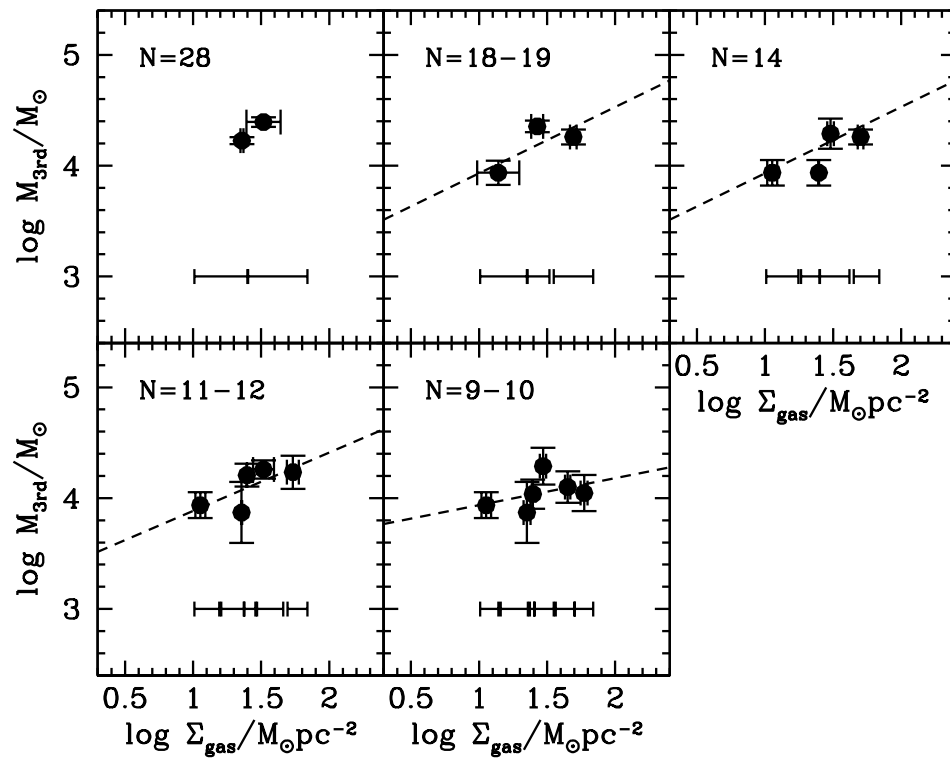


Fig. 6.— M 51, burst 5 Myr ago,  $\log_{10}$  cluster mass versus  $\log_{10}$  total gas surface density, in bins with equal number of clusters. Symbols as in figure 1.

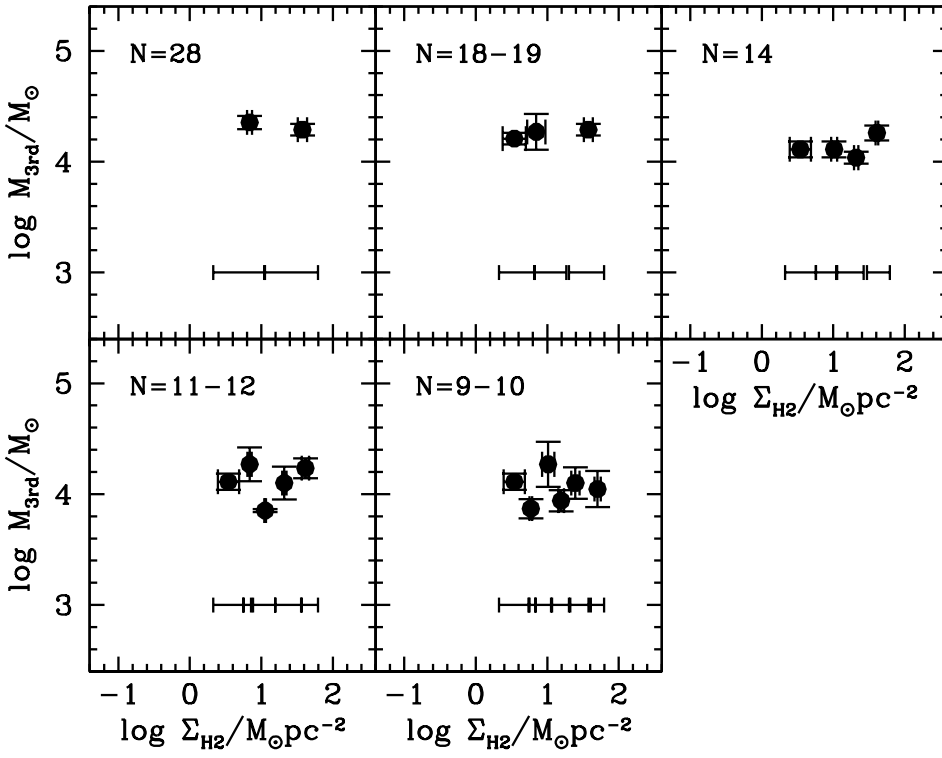


Fig. 7.— M 51, burst 5 Myr ago,  $\log_{10}$  cluster mass versus  $\log_{10}$  molecular gas surface density. Symbols as in figure 1.

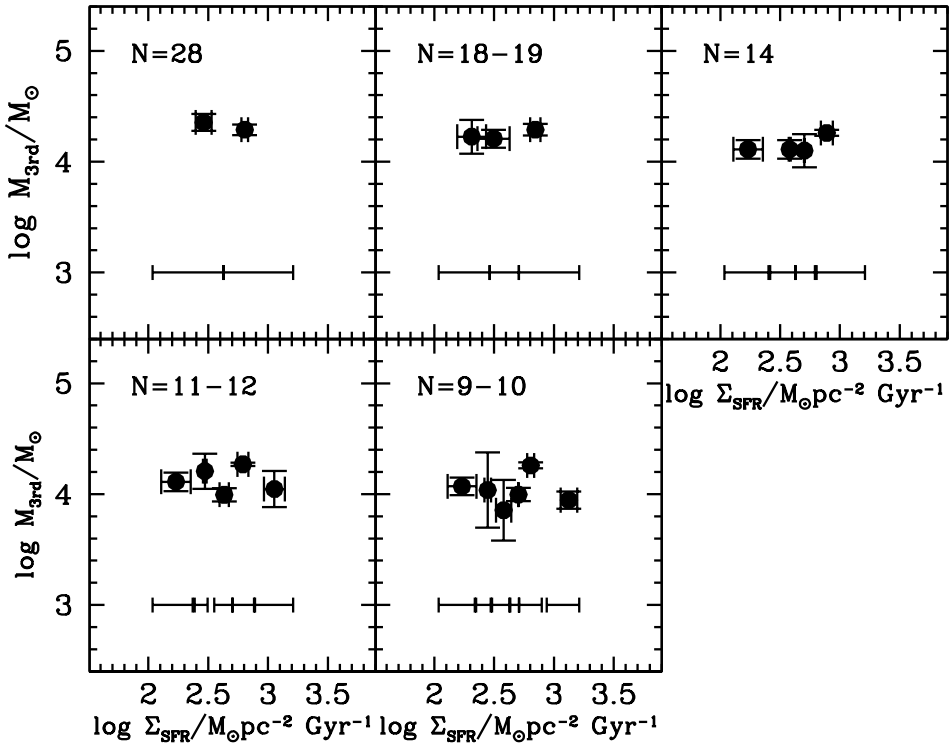


Fig. 8.— M 51, burst 5 Myr ago,  $\log_{10}$  cluster mass versus  $\log_{10}$  star formation rate surface density. Symbols as in figure 1.

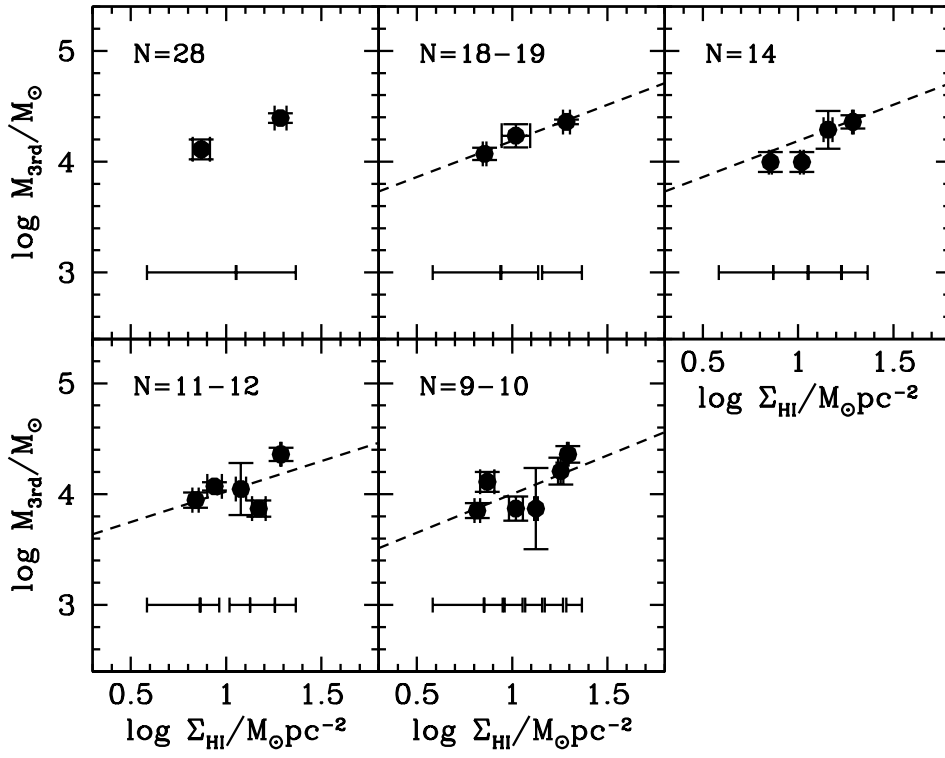


Fig. 9.— M 51, burst 5 Myr ago,  $\log_{10}$  cluster mass versus  $\log_{10}$  neutral gas surface density. *Dashed line:* linear fit. Other symbols as in figure 1.

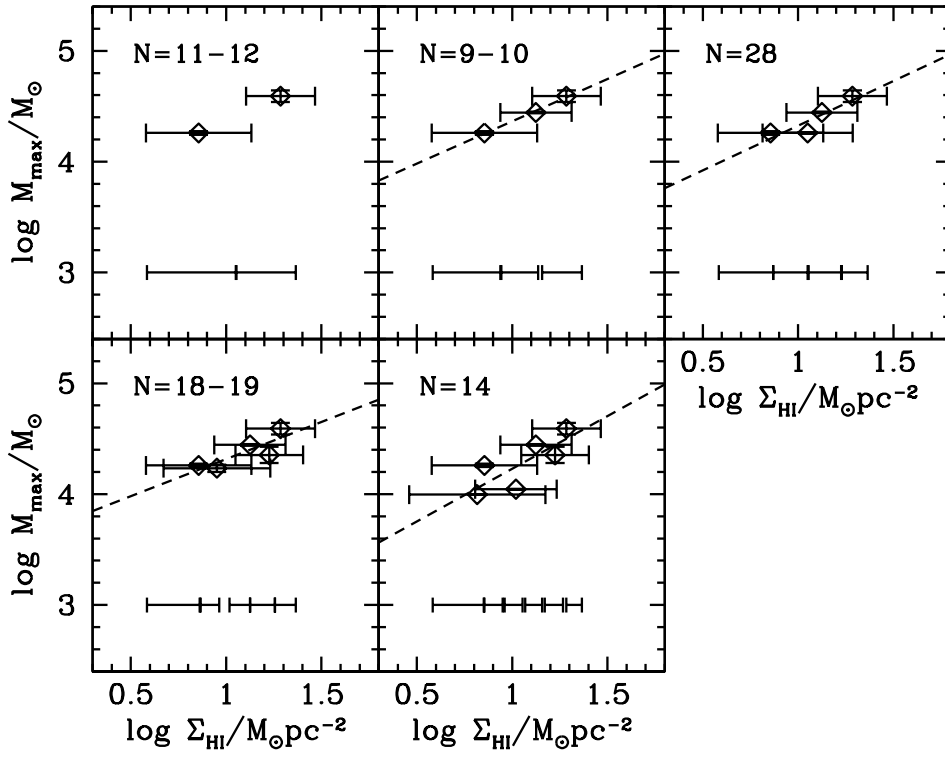


Fig. 10.— M 51, burst 5 Myr ago,  $\log_{10}$  cluster mass versus  $\log_{10}$  neutral gas surface density. *Empty diamonds*: maximum cluster mass; *dashed line*: linear fit. Other symbols as in figure 1.

TABLE 3

M 51, BURST 5 MYR AGO. FITS TO  $\log_{10} (M/M_{\odot})$  VS.  $\log_{10} \Sigma$ ,  $\beta'_x$  AND  $\alpha'_x$ 

$N_b$	$N_{cl}$	$\beta'_{HI}$	$\alpha'_{HI}$
$\log_{10} (M_{3rd}/M_{\odot})$ vs $\Sigma_{HI}/M_{\odot} \text{ pc}^{-2}$			
3	18-19	$(0.7 \pm 0.1)$	$(3.5 \pm 0.1)$
4	14	$(0.7 \pm 0.1)$	$(3.5 \pm 0.1)$
5	11-12	$(0.6 \pm 0.5)$	$(3.5 \pm 0.6)$
6	9-10	$(0.7 \pm 0.4)$	$(3.3 \pm 0.4)$
$\log_{10} (M_{3rd}/M_{\odot})$ vs $\Sigma_{gas}/M_{\odot} \text{ pc}^{-2}$			
3	18-19	$(0.6 \pm 0.5)$	$(3.3 \pm 0.8)$
4	14	$(0.6 \pm 0.5)$	$(3.3 \pm 0.8)$
5	11-12	$(0.5 \pm 0.3)$	$(3.4 \pm 0.4)$
6	9-10	$(0.2 \pm 0.3)$	$(3.7 \pm 0.4)$
$\log_{10} (M_{max}/M_{\odot})$ vs $\Sigma_{HI}/M_{\odot} \text{ pc}^{-2}$			
3	18-19	$(0.8 \pm 0.1)$	$(3.6 \pm 0.1)$
4	14	$(0.8 \pm 0.3)$	$(3.5 \pm 0.3)$
5	11-12	$(0.7 \pm 0.3)$	$(3.6 \pm 0.3)$
6	9-10	$(1.0 \pm 0.4)$	$(3.3 \pm 0.4)$

NOTE.—Col. (1): number of bins. Col. (2): number of clusters in each bin. Col. (3): best-fit slope (eq. 1). Col. (4): best-fit intercept (eq. 1).

TABLE 4  
K-S TEST  $D$  AND  $P$  VALUES, BURST 5 MYR AGO

	$D$	$P$								
Bin	2		3		4		5		6	
1	1.20	0.1108	0.91	0.3754	0.60	0.8646	0.83	0.4892	1.38	0.0438
2			1.12	0.1617	1.12	0.1617	0.81	0.5305	0.78	0.5732
3					0.51	0.9575	0.76	0.6030	1.27	0.0778
4							0.51	0.9575	1.27	0.0778
5									0.76	0.6030

NOTE.— $D$  and  $P$  values for bin pairs. The cell in the intersection of a row  $j$  and a column  $k$  contains the  $D_{j,k}$  and  $P_{j,k}$  parameters, respectively, of the comparison between the two bins indicated in the corresponding row and column. If  $P_{j,k} < 0.05$ , the null hypothesis that the clusters in the two bins are taken from the same mass distribution function is rejected.

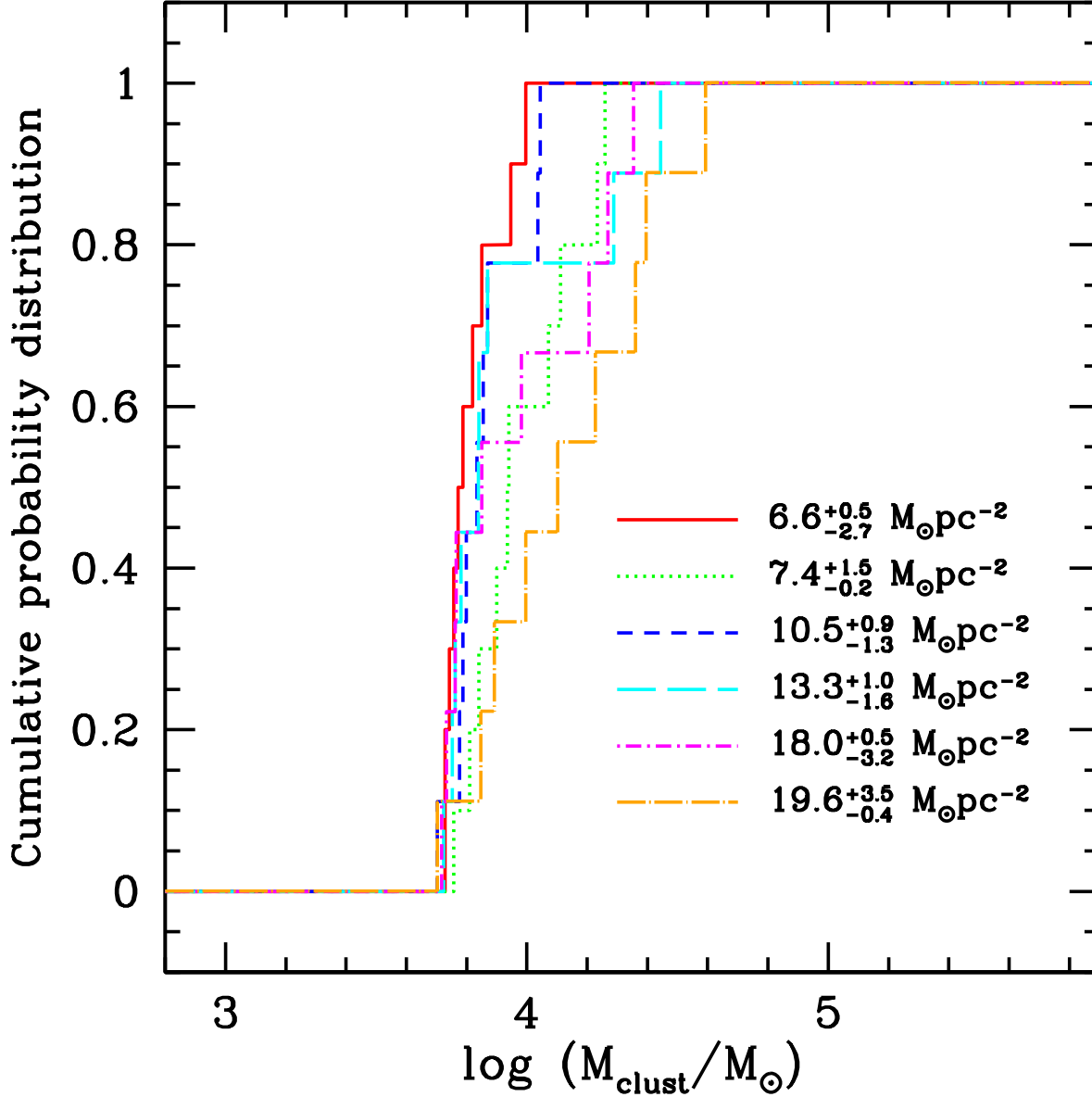


Fig. 11.— K-S test, burst 5 Myr ago. Cumulative probability distributions of mass for clusters in recent burst with  $M_{\text{clust}} \geq 5 \times 10^3 M_{\odot}$  in the six indicated bins of HI surface density. *Red solid line*: bin 1,  $\Sigma_{\text{HI}} = 6.6^{+0.5}_{-2.7} M_{\odot} \text{pc}^{-2}$ ; *green dotted line*: bin 2,  $\Sigma_{\text{HI}} = 7.4^{+1.5}_{-0.2} M_{\odot} \text{pc}^{-2}$ ; *blue short dashed line*: bin 3,  $\Sigma_{\text{HI}} = 10.5^{+0.9}_{-1.3} M_{\odot} \text{pc}^{-2}$ ; *cyan long dashed line*: bin 4,  $\Sigma_{\text{HI}} = 13.3^{+1.0}_{-1.6} M_{\odot} \text{pc}^{-2}$ ; *magenta short dashed-dotted line*: bin 5,  $\Sigma_{\text{HI}} = 18.0^{+0.5}_{-3.2} M_{\odot} \text{pc}^{-2}$ ; *orange long dashed-dotted line*: bin 6,  $\Sigma_{\text{HI}} = 19.6^{+3.5}_{-0.4} M_{\odot} \text{pc}^{-2}$ .

the largest surface density  $\Sigma_{\text{HI}} = 19.6_{-0.4}^{+3.5} M_{\odot} \text{pc}^{-2}$  ( $P_{1,6} = 0.04$ ). The mass distributions in all the other bins lie in between, although we notice that the distributions in bins 4 (*cyan long dashed line*) and 5 (*magenta dashed-dotted line*) are actually closer to bin 1 than to bin 6 ( $P_{1,4} = 0.86$ ;  $P_{4,6} = 0.08$ ;  $P_{1,5} = 0.49$ ;  $P_{5,6} = 0.08$ ).

### 4.3. Comparison with M 33

In a companion paper (González-Lópezlira et al. 2012), we have performed a similar analysis on the flocculent galaxy M 33, except that we have compared the *radial* profiles of cluster mass distribution and gas surface densities. Since M 33 is a flocculent galaxy without a strong spiral perturbation, in general one can assume that the  $\Sigma$  azimuthal averages provide a good estimate of the actual surface densities at any given point located at the same galactocentric distance. From the radial analysis, and both the average and median of the 5 most massive clusters in data bins, we derive for M 33:  $\log_{10} M_{\text{mean},3\text{rd}} \propto (4.7 \pm 0.4) \log_{10} \Sigma_{\text{gas}}$ ;  $\log_{10} M_{\text{mean},3\text{rd}} \propto (1.3 \pm 0.1) \log_{10} \Sigma_{\text{H}_2}$ ;  $\log_{10} M_{\text{mean},3\text{rd}} \propto (1.0 \pm 0.1) \log_{10} \Sigma_{\text{SFR}}$ . One would also derive  $\log_{10} M_{\text{mean},3\text{rd}} \propto (9.6 \pm 1.2) \log_{10} \Sigma_{\text{HI}}$ , but there is a very small range of  $\Sigma_{\text{HI}}$  values in the disk of M 33, as the radial distribution of neutral gas has  $d \Sigma_{\text{HI}}/dR_{25} \approx 0.2 M_{\odot} \text{pc}^{-2} R_{25}^{-1}$  (exponential scale length  $h_{\text{R}} = 4.3 R_{25}$ ), i.e., it is more than twice as shallow as in M 51, which has  $h_{\text{R}} = 2 R_{25}$ .

Here, we present the M 33 data in a way that is directly comparable to our analysis of M 51. To this end, and since all ISM phases have roughly exponential profiles, we use radius as a proxy for surface density, and produce plots for M 33 analogous to Figures 1, 2, 3, and 4. We note that the  $\log_{10} \Sigma$  ranges indicated by the bars at the bottom of the panels sometimes overlap slightly, owing to the departures of the surface density profiles from a perfect exponential; and (2) we omit in all cases the last bin, i.e., the one at the largest galactocentric distance. As explained in González-Lópezlira et al. (2012), this bin is dominated by the most massive cluster in the galaxy, whose formation conditions are badly misrepresented by the azimuthally averaged gas surface density. Moreover, the last bin always includes a radial range for which there is no gas data; these stop at  $\approx 0.85 R_{25}$ . The results of this exercise are

shown in Figures 12, 13, 14, and 15, and in Table 3. Firstly, this fresh look at the data highlights that a correlation does not seem to exist between  $M_{3\text{rd}}$  and  $\Sigma_{\text{HI}}$ .<sup>9</sup> As for the other ISM components, we get:  $\log_{10} M_{3\text{rd}} = (3.8 \pm 0.3) \log_{10} \Sigma_{\text{gas}} + (0.7 \pm 0.3)$ ;  $\log_{10} M_{3\text{rd}} = (1.2 \pm 0.1) \log_{10} \Sigma_{\text{H}_2} + (3.8 \pm 0.1)$ ;  $\log_{10} M_{3\text{rd}} = (0.9 \pm 0.1) \log_{10} \Sigma_{\text{SFR}} + (4.2 \pm 0.1)$ .

The 2-D correlation of  $\log_{10} M_{3\text{rd}}$  with total gas surface density,  $\log_{10} \Sigma_{\text{gas}}$ , has a slightly shallower slope than the comparison between radial profiles. The radial and 2-D results for molecular gas and star formation rate densities, on the other hand, are consistent within  $1 \sigma$ .

## 5. Summary and conclusions

We have analyzed the relationship between maximum cluster mass and gas surface density in M 51, in order to explore the suggestion that maximum cluster mass is determined by physical processes, e.g., the equilibrium pressure between cluster forming cores and the ambient interstellar medium (Larsen 2002; Billett et al. 2002), and since the existence of such a relationship can reconcile SFR measurements derived, respectively, from H $\alpha$  and FUV emission in galaxy disks. Furthermore, we have already found evidence in M 33 that star formation is not a stochastic process, and that the range of star cluster masses is driven by environmental physics.

In our work, we have used published gas data of M 51 (Rots et al. 1990; Schuster et al. 2007; Fletcher et al. 2011), and catalogs originally comprising more than 1800 young star clusters in its disk, also from the literature (Hwang & Lee 2008, 2010). Among other information, these catalogs provide positions, ages, reddenings, and masses for the clusters.

We have compared the 2-D distribution of the young star clusters with those of gas surface density and star formation rate. To test whether any trend is caused by random sampling from the cluster mass function as a size of sample effect, we have measured the distribution of maximum mass with gas surface density in 2 to 6 bins with an equal number of clusters in each bin.

<sup>9</sup>Notice also that the bars at the bottom of Figure 15 overlap more than a little, a sign that  $\Sigma_{\text{HI}}$  is far from changing monotonically with radius.

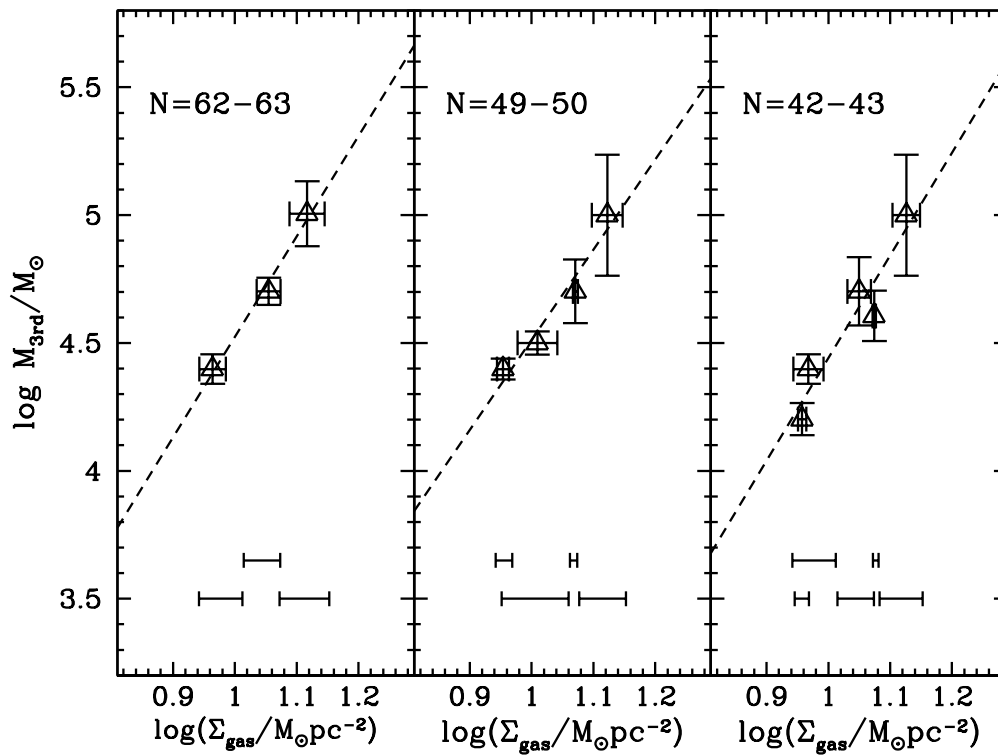


Fig. 12.— M 33,  $\log_{10}$  mass of third most massive cluster vs.  $\log_{10}$  total gas surface density. *Empty triangles*:  $M_{3rd}$ , median of 5 most massive clusters in bin. *Dashed line*: linear fit. Other symbols as in Figure 1.

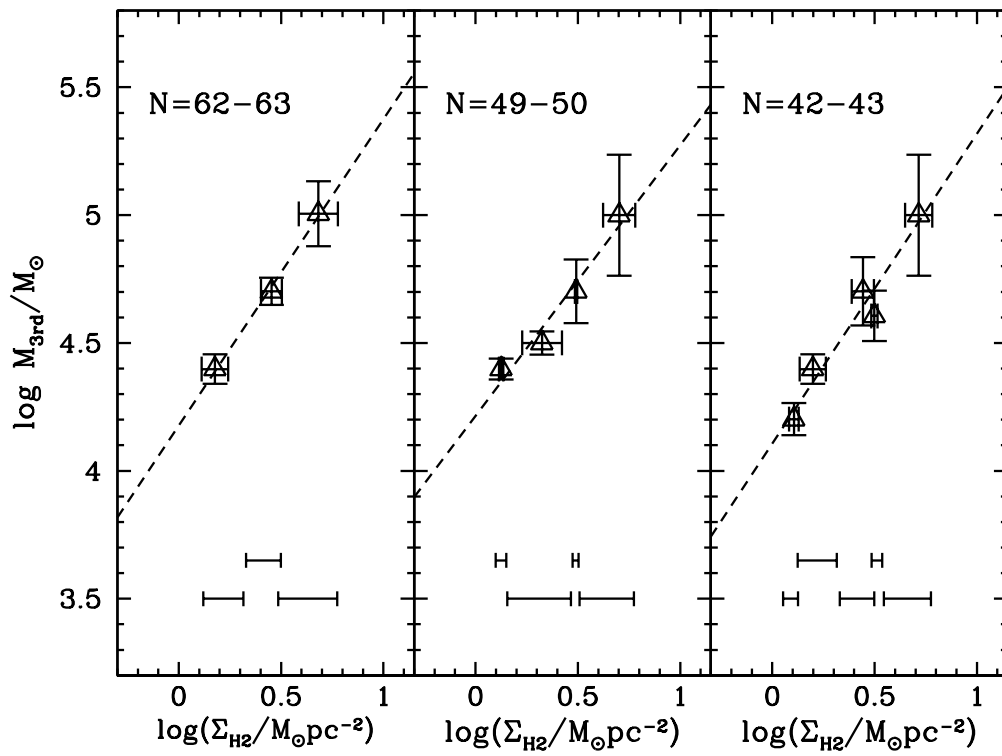


Fig. 13.— M 33,  $\log_{10}$  mass of third most massive cluster vs.  $\log_{10}$  molecular gas surface density. Symbols as in Figure 12.

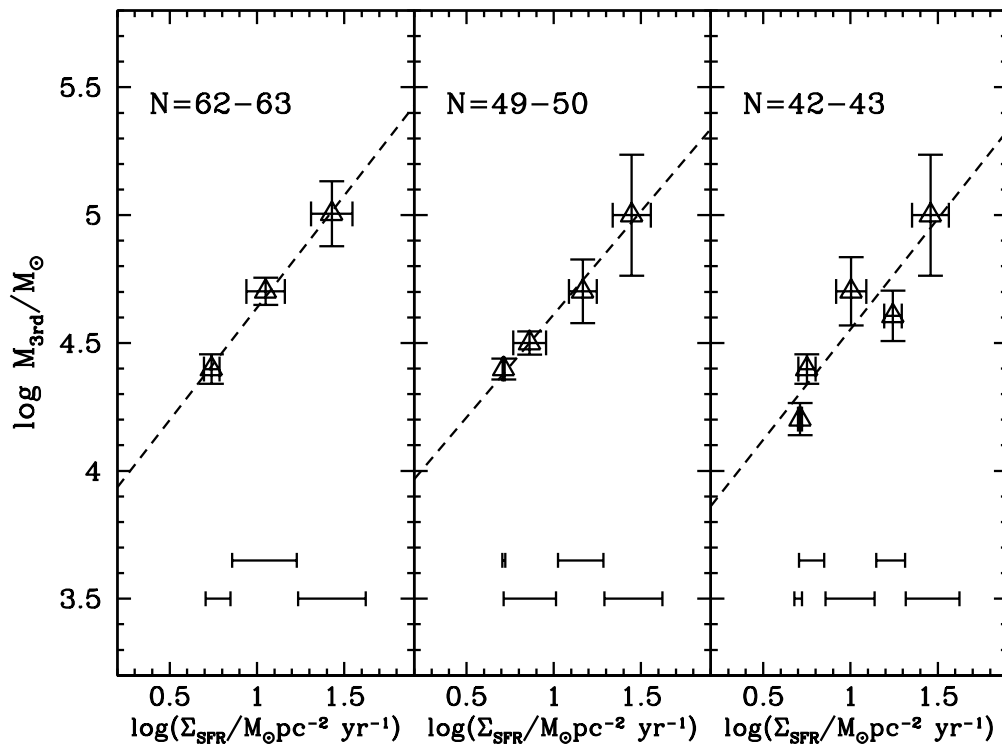


Fig. 14.— M 33,  $\log_{10}$  mass of third most massive cluster vs.  $\log_{10}$  SFR surface density. Symbols as in Figure 12

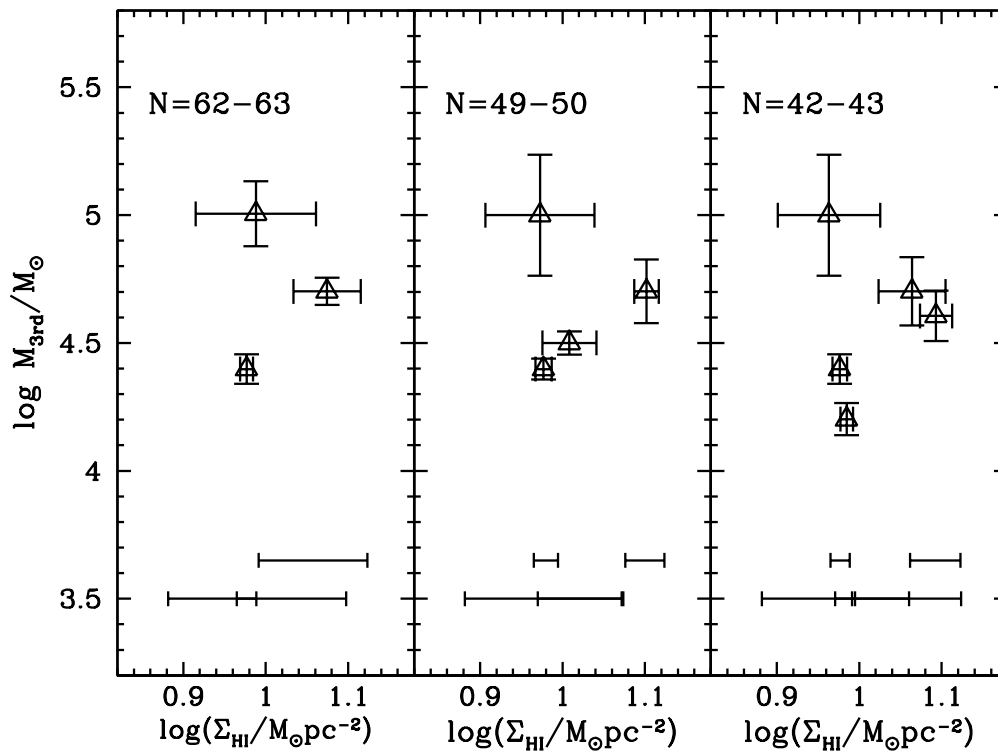


Fig. 15.— M 33,  $\log_{10}$  mass of third most massive cluster vs.  $\log_{10}$  neutral gas surface density. Symbols as in Figure 12

TABLE 5

M 33. FITS TO  $\log_{10} (M_{3\text{rd}}/M_{\odot})$  VS.  $\log_{10} \Sigma$ ,  $\beta'_x$  AND  $\alpha'_x$ 

$N_b$	$N_{\text{cl}}$	$\beta'_x$	$\alpha'_x$
$\Sigma_{\text{gas}}/M_{\odot} \text{ pc}^{-2}$			
3	62-63	$(3.9 \pm 0.4)$	$(0.6 \pm 0.4)$
4	49-50	$(3.5 \pm 0.6)$	$(1.0 \pm 0.6)$
5	42-43	$(4.0 \pm 0.8)$	$(0.4 \pm 0.8)$
$\Sigma_{\text{H}_2}/M_{\odot} \text{ pc}^{-2}$			
3	62-63	$(1.2 \pm 0.1)$	$(4.18 \pm 0.03)$
4	49-50	$(1.1 \pm 0.2)$	$(4.2 \pm 0.1)$
5	42-43	$(1.2 \pm 0.2)$	$(4.1 \pm 0.1)$
$\Sigma_{\text{SFR}}/M_{\odot} \text{ pc}^{-2} \text{ Gyr}^{-1}$			
3	62-63	$(0.9 \pm 0.1)$	$(3.8 \pm 0.1)$
4	49-50	$(0.8 \pm 0.1)$	$(3.8 \pm 0.1)$
5	42-43	$(0.9 \pm 0.2)$	$(3.7 \pm 0.2)$

NOTE.—Col. (1): number of bins. Col. (2): number of clusters in each bin. Col. (3): best-fit slope (eq. 1). Col. (4): best-fit intercept (eq. 1).

We examined two samples of clusters in M 51: one of 167 clusters 25 to 400 Myr old, and with a mass of at least  $1 \times 10^5 M_{\odot}$ , and another one of 56 clusters younger than 10 Myr, with masses of 5000  $M_{\odot}$  and up. For the older sample, regardless of the number of bins, we find no correlation between the mass of the 3rd most massive cluster in each bin,  $M_{3\text{rd}}$ , and the local surface densities of total gas, molecular gas, or star formation rate. There is, however, a hint of a correlation with local neutral gas surface density, such that  $\log_{10} M_{3\text{rd}} = (0.4 \pm 0.2) \log_{10} \Sigma_{\text{HI}} + (5.2 \pm 0.3)$ .

For the younger sample, we find no correlation between  $M_{3\text{rd}}$ , and either  $\Sigma_{\text{H}_2}$  or  $\Sigma_{\text{SFR}}$ . On the other hand, there is a correlation with  $\Sigma_{\text{HI}}$  that is tighter and with a slightly steeper slope than the one found for old sample (although still consistent with it):  $\log_{10} M_{3\text{rd}} = (0.6 \pm 0.1) \log_{10} \Sigma_{\text{HI}} + (3.5 \pm 0.1)$ . A correlation may also exist for the most recent burst of  $M_{3\text{rd}}$  with the total mass surface density  $\Sigma_{\text{gas}}$ :  $\log_{10} M_{3\text{rd}} = (0.5 \pm 0.2) \log_{10} \Sigma_{\text{gas}} + (3.4 \pm 0.2)$ . If true, the comparison between the correlations with the older and younger burst implies that the normalization depends on the cluster mass and/or age ranges.

The results could not be more different from the ones obtained for the flocculent galaxy M 33. From a 1-D radial analysis, we have previously derived for M 33:  $M_{3\text{rd}} \propto \Sigma_{\text{gas}}^{4.7 \pm 0.4}$ ;  $M_{3\text{rd}} \propto \Sigma_{\text{H}_2}^{1.3 \pm 0.1}$ ;  $M_{3\text{rd}} \propto \Sigma_{\text{SFR}}^{1.0 \pm 0.1}$ . With a treatment that mimicks the 2-D analysis of M 51, we get for M 33:  $M_{3\text{rd}} \propto \Sigma_{\text{gas}}^{3.8 \pm 0.3}$ ;  $M_{3\text{rd}} \propto \Sigma_{\text{H}_2}^{1.2 \pm 0.1}$ ;  $M_{3\text{rd}} \propto \Sigma_{\text{SFR}}^{0.9 \pm 0.1}$ .

In M 33, the relation between  $M_{3\text{rd}}$  and  $\Sigma_{\text{SFR}}$  is consistent with the expectations from pressure equilibrium considerations. On the other hand, the slope of the correlation with  $\Sigma_{\text{gas}}$  is steeper than the value assumed by Pflamm-Altenburg & Kroupa (2008) to explain the H $\alpha$  cut-off in galaxy disks. There is no correlation with  $\Sigma_{\text{HI}}$ , but M 33 is known to have been interacting, and the HI distribution may not reflect the equilibrium configuration. The tight correlation with  $\Sigma_{\text{H}_2}$  and  $\Sigma_{\text{SFR}}$ , and the looser one with  $\Sigma_{\text{gas}}$  agree with the recent results of a study of 33 nearby spiral galaxies by Schrubba et al. (2011), who find a tight and linear relation between  $\Sigma_{\text{SFR}}$  and  $\Sigma_{\text{H}_2}$ , with little dependence on  $\Sigma_{\text{gas}}$ .

How can one understand the diametrically opposite results found for the grand-design spiral M 51? It is, of course, possible that stochastic

sampling is at work in M 51, such that the most massive cluster masses scale with the size of the sample. But then we would have to accept that stochastic sampling operates in some cases, like in M 51, and not in others, like in M 33.

We propose a different hypothesis. The large azimuthal variations in gas and SFR surface densities in M 51 preclude a radial approach. Instead, we compared star cluster masses with local surface densities. The problem then is that, typically, the clusters detected in the ACS data with masses above the completeness limit of  $10^5 M_\odot$  are older than  $10^8$  yr (only 24 out of 167 have ages between 40 and 90 Myr). Even if the cluster mass function is approximately independent of age over a timescale of a few hundred million years, clusters also complete between half and two full orbits around the galaxy in this time, and hence the local gas density around any given cluster probably has little to do with the gas density at the site and time of cluster formation.

The two facts, that the correlation between  $M_{3rd}$  and  $\Sigma_{HI}$  seems to be tighter for the younger sample, and that this latter group of clusters might also exhibit a correlation between cluster mass and total gas surface density  $\Sigma_{gas}$ , give some credibility to this hypothesis. Unfortunately, the resolution of the radio data implies that we are comparing clusters with sizes of the order of 10 pc with gas surface densities averaged over an area of  $\approx 750 \times 750$  pc<sup>2</sup>. Even in the case of the younger sample, the measured  $\Sigma$ s are likely quite diluted compared to the actual densities relevant for the formation of the clusters.

By contrast, 257 out of the 258 clusters kept for the final analysis in M 33 are younger than  $2.5 \times 10^7$  yr (the age of the exception is 60 Myr) and, at any rate, the lack of a strong spiral perturbation means that the azimuthally averaged gas emission is in general representative of the star-forming conditions of clusters located at the same radii.

To be able to perform a statistically significant analysis of clusters younger than 25 Myr, still close to their birthsites and whose local gas densities resemble their star-forming environments, the depth and resolution of the cluster data need to be enough for the assembly of a sufficiently numerous sample above the mass function completeness

limit.<sup>10</sup> The gas data should also have a resolution comparable to the physical sizes of the clusters.

The confirmation of the M 33 results will have to wait for the outcome of studies in closer targets, like the Magellanic Clouds, where the mass density distribution of clusters younger than a few  $\times 10^7$  yr can be probed with large numbers down to 100-1000  $M_\odot$ , and where the clusters' physical sizes are well matched by the resolution achievable at radio wavelengths; the data to do so already exist.

RAGL is grateful for the support received from DGAPA, UNAM, and CONACyT, Mexico. N. Hwang and M. G. Lee generously provided the cluster catalogs used in this work. We thank A. Rots, K. Schuster, and R. Beck for granting access to the HI, CO, and 20 cm continuum images of M 51, respectively. L. Loinard helped with the nitty gritty details of the conversion of the reduced radio data to physical surface densities, and with the transformation of the HI image to coordinates J2000. We acknowledge the positive and helpful comments of an anonymous referee.

## REFERENCES

- Billett, O. H., Hunter, D. A., & Elmegreen, B. G. 2002, *AJ*, 123, 1454
- Bruzual, G., & Charlot, S. 2003, *MNRAS*, 344, 1000
- Chandar, R., Whitmore, B. C., Calzetti, D., et al. 2011, *ApJ*, 727, 88
- Chandar, R., Whitmore, B. C., Kim, H., et al. 2010, *ApJ*, 719, 966
- Corbelli, E. 2003, *MNRAS*, 342, 199
- Fall, S. M., Chandar, R., & Whitmore, B. C. 2009, *ApJ*, 704, 453
- Feldmeier, J. J., Ciardullo, R., & Jacoby, G. H. 1997, *ApJ*, 479, 231

<sup>10</sup>Number of clusters increases with decreasing mass. On the other hand, the absolute number of the most massive, easily detectable, clusters will grow as generations of star formation accumulate. Hence, the majority of massive clusters in a galaxy, even with active star formation, will be old, whereas for this project it is best to work only with the most recent bursts.

Fletcher, A., Beck, R., Shukurov, A., Berkhuijsen, E. M., & Horellou, C. 2011, *MNRAS*, 412, 2396

González-Lópezlira, R. A., Pflamm-Altenburg, J., & Kroupa, P. 2012, *ApJ*, 761, 124

Hartmann, L., Ballesteros-Paredes, J., & Bergin, E. A. 2001, *ApJ*, 562, 852

Helou, G., Soifer, B. T., & Rowan-Robinson, M. 1985, *ApJ*, 298, L7

Heyer, M. H., Corbelli, E., Schneider, S. E., & Young, J. S. 2004, *ApJ*, 602, 723

Hwang, N., & Lee, M. G. 2008, *AJ*, 135, 1567

Hwang, N., & Lee, M. G. 2010, *ApJ*, 709, 411

Israel, F., & Rowan-Robinson, M. 1984, *ApJ*, 283, 81

Kennicutt, R. C., Jr. 1998, *ARA&A*, 36, 189

Larsen, S. S. 2002, *AJ*, 124, 1393

Larsen, S. S. 2004, *A&A*, 416, 537

Lee, M. G., Chandar, R., & Whitmore, B. C. 2005, *AJ*, 130, 2128

Parmentier, G., & de Grijs, R. 2008, *MNRAS*, 383, 1103

Pflamm-Altenburg, J., & Kroupa, P. 2008, *Nature*, 455, 641

Pflamm-Altenburg, J., Weidner, C., & Kroupa, P. 2009, *MNRAS*, 395, 394

Rickard, L. J., Turner, B. E., & Palmer, P. 1977, *ApJ*, 218, L51

Rosa-González, D., Terlevich, E., & Terlevich, R. 2002, *MNRAS*, 332, 283

Rots, A. H., Bosma, A., van der Hulst, J. M., Athanassoula, E., & Crane, P. C. 1990, *AJ*, 100, 387

Schruba, A., Leroy, A. K., Walter, F., et al. 2011, *AJ*, 142, 37

Schuster, K. F., Kramer, C., Hitschfeld, M., Garcia-Burillo, S., & Mookerjea, B. 2007, *A&A*, 461, 143

Silk, J. 1997, *ApJ*, 481, 703